Novel amiloride derivatives that inhibit bacterial motility across multiple strains and stator types

MI Islam[1]*, JH Bae[1]*, T Ishida[2*], P Ridone[1], J Lin[1], MJ Kelso[3,4], Y Sowa[2,5], BJ Buckley[3,4], MAB Baker[1,6].

*joint contribution – joint author names are listed in order of chronological involvement in this project.

1. School of Biotechnology and Biomolecular Sciences, University of New South Wales, Sydney, NSW 2052, Australia.
2. Department of Frontier Bioscience, Hosei University, Tokyo, Japan.
3. Molecular Horizons and School of Chemistry and Molecular Bioscience, University of Wollongong, Wollongong, NSW 2522, Australia
4. Illawarra Health and Medical Research Institute, Wollongong, NSW 2522, Australia.
5. Research Center for Micro-Nano Technology, Hosei University, Tokyo, Japan.
6. CSIRO Synthetic Biology Future Science Platform, Brisbane, Australia.
Correspondence: matthew.baker@unsw.edu.au

Keywords:

Bacterial motility, bacterial flagellar motor, amiloride, sodium channel blocker, stator.

Abstract:

The bacterial flagellar motor (BFM) is a protein complex that confers motility to cells and contributes to survival and virulence. The BFM consists of stators that are ion-selective membrane protein complexes and a rotor that directly connects to a large filament, acting as a propeller. The stator complexes couple ion transit across the membrane to torque that drives rotation of the motor. The most common ion gradients that drive BFM rotation are protons (H^+) and sodium ions (Na^+). The sodium-powered stators, like those in the PomAPomB stator complex of Vibrio spp, can be inhibited by sodium channel inhibitors, in particular, by phenamil, a potent and widely used inhibitor. However, relatively few new sodium-motility inhibitors have been described since the discovery of phenamil. In this study, we characterised two possible motility inhibitors HM2-16F and BB2-50F from a small library of previously reported amiloride derivatives. We used three approaches: effect on rotation of tethered cells, effect on free swimming bacteria and effect on rotation of marker beads. We showed that both HM2-16F and BB2-50F stopped rotation of tethered cells driven by Na^+ motors comparable to phenamil at matching concentrations, and could also stop rotation of tethered cells driven by

36 H^+ motors. Bead measurements in presence and absence of stators confirmed that the
37 compounds did not inhibit rotation via direct association with the stator, in contrast to the
38 established mode of action of phenamil. Overall, HM2-16F and BB2-50F stopped swimming
39 in both Na^+ and H^+ stator types, and in pathogenic and non-pathogenic strains.
40
41 **Importance:**
42 Here we characterised two novel amiloride derivatives in the search for antimicrobial
43 compounds that target bacterial motility. Our two compounds were shown to inhibit flagellar
44 motility at 10 μM across multiple strains, from non-pathogenic *E. coli* with flagellar rotation
45 driven by proton or chimeric sodium-powered stators, to proton-powered pathogenic *E. coli*
46 (EHEC/UPEC) and lastly in sodium-powered *Vibrio alginolyticus*. Broad anti-motility
47 compounds such as these are important tools in our efforts control virulence of pathogens in
48 health and agricultural settings.
49
50 **Introduction:**
51 Motility is essential for many bacteria to find nutrients and escape unfavourable conditions (1).
52 Bacterial cells move through liquids or over moist surfaces using rotating flagella, which are
53 driven by the bacterial flagellar motor (BFM) (2). In peritrichous bacteria such as *E. coli*, when
54 the majority of BFMs rotate counter-clockwise, bacteria move linearly (i.e., run) and when one
55 or more BFM rotates clockwise, the helical filament-bundle unravels and bacteria change
56 direction (i.e., tumble) (3). The BFM contains the stator proteins (e.g., MotA and MotB in *E.*
57 *coli* and PomA and PomB in *Vibrio* spp.), which form an ion transporter on the inner cell
58 membrane, and the rotor proteins (e.g., FliG, FliM, and FliN), that are driven to rotate by torque
59 generation between the stator and rotor (4). Rotation of the BFM is powered by translocation
60 of specific ions (e.g., H^+ in *E. coli* and Na^+ in *Vibrio* spp.) across the cell membrane through
61 the stator complex (4).
62 Beside locomotion, motility is crucial during the initial infection and colonisation processes of
63 different pathogenic bacteria (5). Locomotion reduces repulsion between the bacterial cell wall
64 and host tissues, promoting attachment to host cells (6). The importance of motility as a
65 virulence factor was first noted in *Campylobacter jejuni,* when only the motile strain of *C.*
66 *jejuni* was recovered from an infection site where a mixture of motile and non-motile *C. jejuni*
67 phase variants were used to initiate infection (7). It has since been demonstrated that flagellum-
68 mediated motility promotes the virulence of several gram-negative pathogens, such as for
69 *Bordetella bronchiseptica, B. pertussis* (8)*, Helicobacter sp.* (9)*, Legionella pneumophila* (10),

70 pathogenic *E. coli* strains (11), *Pseudomonas aeruginosa* (12), *Salmonella typhimurium* (13),
71 and *Vibrio cholerae* (14). Aside from host attachment, flagella also contribute to the formation
72 of biofilms by multiple bacterial pathogens, which promote the development of persistent and
73 chronic infections and antibiotic resistance (1).
74 Amiloride is a diuretic drug and well-characterised inhibitor of the Na^+ bacterial flagellar motor
75 (15). Amiloride inhibits rotation of the sodium-powered flagellar motor by blocking the
76 translocation of Na^+ ions through the channel in a competitive and rapidly reversible manner
77 (16). However, amiloride is of limited utility due to its weak anti-motility activity and adverse
78 effects on other metabolic processes (17). The *N*-phenyl substituted amiloride analogue,
79 phenamil, has been identified as a better inhibitor of sodium-powered flagellar motors (17).
80 Phenamil is markedly more potent than amiloride and shows non-competitive inhibition of
81 bacterial motility with slow dissociation (18). Phenamil stops flagellar rotation by binding to a
82 site predicted to lie at the cytoplasmic face of the PomAPomB stator complex (19). Phenamil
83 is a useful tool for flagellar research, but requires high concentrations (>20 μM) and resistant
84 stators can arise from a single point mutation (20, 21). More potent and specific compounds
85 may assist research into stator function and potentially offer leads for new antivirulence drugs.
86 While classical uncouplers can be used to inhibit proton-powered motors, they also have
87 adverse effects on cells resulting from collapse of the membrane potential. For example the
88 commonly used uncoupler, carbonyl cyanide *m*-chlorophenyl hydrazone (CCCP), is toxic to
89 both prokaryote and eukaryote cells (22). Here, we report that two recently reported 6-
90 substituted amiloride analogues, BB2-50F and HM2-16F(23, 24) (Fig. 1A), inhibit motility in
91 known phenamil-resistant strains and affect both Na^+- and H^+-powered flagellar motors.
92
93 **Results:**
94 ***Inhibition of motility***
95 We initially evaluated the anti-motility activity of BB2-50F and HM2-16F (Fig. 1A) along with
96 the control compounds 5-(*N*,*N*-hexamethylene)amiloride (HMA) and phenamil using a
97 tethered cell assay (Fig. 1B). We examined the effect of each compound on rotational speed at
98 increasing concentrations (0, 1, 10 and 100 μM) against Na^+-powered stator, PomAPotB in *E.*
99 *coli* SYC35 (Δ*motAmotB fliC*^{sticky}) strains. Both BB2-50F and HM2-16F inhibited rotation
100 speed in a dose-dependent manner and showed complete inhibition at 10 μM and above (Fig.
101 1B). The positive control for Na^+ -inhibition, phenamil showed similar dose-dependency, with
102 complete inhibition at 10 μM (Fig. 1B). HMA was less potent, with 65% of cells still rotating

103 at 10 μM (Fig. 1B), in agreement with previous findings for other 5-substituted amiloride
104 analogues (16).
105 We further characterised the activity of BB2-50F and HM2-16F alongside phenamil over the
106 concentration range 0−10 μM (Fig. 1C). BB2-50F showed a 2% reduction in the number of
107 rotating cells at 1 μM, 4% at 2.5 μM, 12% at 5 μM, 20% at 7.5 μM and 79% at 10 μM (Fig
108 1C). HM2-16F showed a 6% reduction in the number of rotating cells at 1 μM, 15% at 2.5 μM,
109 28% at 5 μM, 62% at 7.5 μM and 100% at 10 μM (Fig. 1C). In comparison, phenamil produced
110 a 27% reduction in the number of rotating cells at 1 μM, 36% at 2.5 μM, 51% at 5 μM, 58% at
111 7.5 μM and 74% at 10 μM (Fig. 1C). The effect of each compound was reversed following
112 washing with motility buffer.
113 ***Effect on bacterial growth***
114 We measured the growth of *E. coli* SYC35 cells expressing sodium-powered stators
115 (PomAPotB) and proton-powered stators (MotAMotB), and on EHEC and UPEC strains in the
116 presence of 10 μM and 100 μM BB2-50F and HM2-16F (Supplementary Fig. 1). The rate of
117 growth in both strains was not inhibited relative to vehicle controls for either HM2-16F or
118 BB2-50F at 10 μM (Supplementary Fig. 1). However, at 100 μM the compounds differed in
119 toxicity. HM2-16F reduced the growth rate relative to control over the first five hours in both
120 strains, but did not significantly decrease growth at 15 h, while BB2-50F completely inhibited
121 growth at 100 μM.
122 ***Effect of Na^+ concentration on motility inhibition***
123 We evaluated the inhibition of rotation for BB2-50F, HM2-16F and phenamil while varying
124 the concentration of external sodium to test for Na^+-competitive effects (17). Compounds were
125 tested at concentrations of 1−10 μM using motility buffers containing 1, 5, 20, and 85 mM Na^+.
126 No significant differences in inhibition were observed for HM2-16F and BB2-50F at the Na^+
127 concentrations tested (Fig. 1D). Inhibition was generally flat for BB2-50F between 0-7.5 μM,
128 with a sharp drop seen at 10 μM, whereas HM2-16F inhibition showed a more gradual effect
129 across the range of concentrations tested. In contrast, an exponential decay was seen for
130 phenamil across the concentration range, with the fitted decay constant indistinguishable at all
131 sodium concentrations (Fig 1D, left).
132 ***Activity against phenamil-resistant variants and the proton powered MotA/MotB complex***
133 To assess whether the inhibition of rotation was affected by point mutations known to confer
134 resistance to phenamil, we tested BB2-50F and HM2-16F against known phenamil-resistant
135 mutant constructs at 1, 10 and 100 μM using the tethered cell assay. Four different stator

136 mutants were tested in SYC35: PomA(D148Y)/PotB, PomA/PotB(P16S),
137 PomA(D148Y)/PotB(P16S) and PomA/PotB(F22Y/L28Q) (68, 69). Phenamil at 10 μM
138 exhibited no significant effect on the resistant strains (Fig. 2A). In contrast, both compounds
139 showed significant inhibition, completely stopping motility at 10 μM in all phenamil-resistant
140 strains (Fig. 2B & C).
141 To further profile the specificity of the inhibitors, we evaluated BB2-50F and HM2-16F against
142 the proton-powered stator complex (MotAMotB) in SYC35. Both HM2-16F and BB2-50F
143 reduced rotation of the proton-powered motor at 10 μM and completely inhibited rotation at
144 100 μM (Fig. 2). In contrast, phenamil did not inhibit MotAMotB stators at concentrations up
145 to 100 μM (Fig. 2).
146 ***Inhibition of motility in other bacterial strains***
147 Inhibition of motility by BB2-50F and HM2-16F was tested in three additional bacterial strains
148 using a free swimming assay that measures the speed of individual cells by videography(25).
149 We first demonstrated inhibition of swimming in MotAMotB and PomAPotB expressing cells
150 (Fig. 3AB), followed by three additional strains: uropathogenic *E. coli* (UPEC)(26) (Fig. 3C),
151 an attenuated enterohemorrhagic *E. coli* (EHEC)(27, 28) (Fig. 3D) and a native sodium
152 swimmer *Vibrio alginolyticus* (29) (Fig. 3E). Both BB2-50F and HM2-16F significantly
153 reduced swimming speed at 10 μM in all strains ($p < 0.05$ in all cases).
154 ***Characterising mechanism of motility inhibition***
155 The activity of BB2-50F and HM2-16F was measured in a bead rotation assay using 1 μm
156 polystyrene bead attached to sticky flagellar filament of JHC36 (Δ*motAmotB* Δ*cheY fliC*^{sticky})
157 (Fig. 4, Supplementary Fig. 2). This approach reduced the potential for confounding factors
158 that may have affected the tethered cell assay, such as cell-surface adhesion, while also
159 allowing examination of rotation at lower load and at higher speed. Phenamil reduced
160 PomAPotB-driven rotation from 98 ± 7 Hz at 0 μM to 7± 3 Hz at 10 μM (Fig. 4A) but had no
161 effect on the proton-powered MotAMotB (Fig. 4D). In contrast, BB2-50F and HM2-16F
162 reduced the rotation speed of both sodium-powered (PomAPotB) and proton-powered
163 (MotAMotB) motors to zero at 10 μM (Fig. 4BCF).
164 To assess whether the effects of HM2-16F or BB2-50F were due to direct targeting of the stator
165 complex, we measured rotational diffusion of the bead in the presence of drug using the
166 statorless strain. This approach allowed interrogation of whether the compounds were targeting
167 another component of the flagellar motor to inhibit rotation such as the LP ring or bushing.
168 Rotational diffusion for statorless cells remained free in the presence of 10 μM phenamil,
169 indicating no effect on non-stator proteins (Fig. 4G). However, the position of the bead was

170 fixed with minimal rotational or spatial diffusion in the presence of 10 μM BB2-50F (Fig.4H)
171 and HM2-16F (Fig. 4I). We confirmed that rotational diffusion of tethered cells was also
172 restricted in the presence of 10 μM of each compound (Supplementary Fig. 3). Overall, these
173 data suggest a difference in the mode of action of HM2-16F and BB2-50F compared to
174 phenamil, as these compounds appeared to lock the rotational movement of a 1 μm polystyrene
175 bead.
176 To reduce the possibility of measurements being influenced by lingering surface effects from
177 these comparatively large beads, we reduced bead size and composition, and thus mechanical
178 load, by using a 60 nm gold-nanoparticle attached directly to a straightened hook (30). Given
179 the smaller size of the gold bead, and the straightened hook, this system removed possible bead-
180 cell interactions that may have influenced the earlier polystyrene bead assays. Furthermore, the
181 gold nanoparticle assay allows precise measurement of rotation speed at a load close to zero,
182 providing more direct measure of rotor/stator dynamics free from signal damping caused by
183 viscous drag and mechanical loading (31, 32). For this experiment, we used plasmids
184 expressing proton-powered stator MotAMotB (either pSYC28 or pSYC409) and the
185 sodium-powered stator PomAPotB (pSHU1234) in SHU174 (Δ*motAmotB* Δ*fliC* Δ*cheY*
186 *flgE*$_{+GSS+3Cys}$ *fliK2798*). The gold nanoparticle measurements indicated that there was no effect
187 of the compounds at 10 μM on motor rotation driven by either stator type (Fig 5). We further
188 examined the effect of 10 μM of BB2-50F and HM2-16F at low load in statorless cells and
189 observed no measurable difference in rotational diffusion (Fig. 5FG).
190 Rotation completely stopped at the 100 μM toxic concentration of BB2-50F for both stator
191 types and for the statorless strains (Supplementary Fig. 4 & 5). In contrast, application of
192 100 μM of HM2-16F showed mixed effects (Supplementary Fig. 4 & 6). Rotation driven by
193 PomAPotB was not affected, however rotation driven by MotAMotB saw reversible stopping
194 (Supplementary Fig. 6C), irreversible stopping (Supplementary Fig. 6D) and no effect
195 (Supplementary Fig. 6E). Likewise, in statorless strains rotational diffusion of gold beads was
196 both reversibly (Supplementary Fig. 6F) and irreversibly (Supplementary Fig. 6G) stopped.
197 These results suggest that at non-toxic concentrations of compound (10 μM) both
198 BB2-50F and HM2-16F do not directly target the bushing or the rod of the BFM. Upon
199 observing this, tethered cell assays were repeated in the presence of 0.002% w/v Tween 20 to
200 test whether detergent could remove possible hydrophobic interactions between the bead and
201 cell surface that might underlie the broad anti-motility effect, however no reduction in drug
202 effect was observed (Supplementary Fig. 7). This showed that the effect of the compounds was
203 not removed by a well-validated detergent (33, 34), screening for non-specific interactions

204 between the bead and cell-surface in the presence of each inhibitor. In contrast, phenamil
205 significantly reduced the rotation speed of PomAPotB containing cells in the gold bead assay
206 at 10 μM (Fig. 5A), in accordance with its direct, non-competitive mode of inhibition described
207 previously.
208
209
210 ***Fluorescence of HM2-16F***
211 We expected HM2-16F in particular to have improved fluorescence properties relative to
212 phenamil due to the additional benzofuran group conjugated to the pyrazine core. We measured
213 excitation and emission spectra (Supplementary Fig. 8A), and imaged cells in epifluorescence
214 to observe staining with 10 μM HM2-16F (Supplementary Fig. 8B). We further tested HM2-
215 16F using lifetime fluorescence imaging as the quantum yield appeared low (unsuitable for
216 single-molecule imaging). We found that the fluorescence lifetime of HM2-16F was 5.4 ± 0.1
217 ns, enabling clear resolution against cellular autofluorescence (1.5 ± 0.1 ns) (Supplementary
218 Fig. 8C).
219
220 **Discussion**
221 Motility is a potential target for new anti-virulence agents (35). Motility inhibitors are expected
222 to exert less selective pressure than current antibiotics (36), and are typically effective at
223 concentrations lower than those needed for the antibacterial effects of conventional antibiotics
224 (37). This approach may allow for more specific pathogen targeting (e.g. sodium only) as well
225 as lower dosage requirements. Amiloride and its analogues are the best known inhibitors of
226 sodium driven bacterial flagellar motors (16, 17, 38, 39). In this study, we evaluated the anti-
227 motility activity of two new amiloride derivatives, BB2-50F and HM2-16F using four sets of
228 experiments: 1) tethered cell rotation; 2) free-swimming, 3) 1 μm bead rotation, and 4) 60 nm
229 gold bead rotation.
230 Sodium-driven bacterial rotation was stopped in tethered cell and 1 μm bead assays at 10 μM
231 for BB2-50F, HM2-16F and phenamil, indicating that these compounds show similar potency.
232 The new compounds showed better anti-motility activity at lower concentrations than other
233 reported motility inhibitors for sodium powered motor system, e.g. amiloride and arginine (16,
234 40). Furthermore, the effect of both BB2-50F and HM2-16F (Fig 1D) appeared to be sodium
235 independent, unlike the Na^+-competitive parent amiloride (17). In addition to its activity at low
236 concentrations, HM2-16F also showed green fluorescence properties relative to phenamil,
237 enabling the use of epifluorescence and lifetime imaging to measure uptake and release of

238 HM2-16F in treated cells (Supplementary Fig. 8). This finding bolsters its potential
239 applications in, for example, infection diagnostics (41).
240 BB2-50F and HM2-16F did not affect cellular growth at the motility-blocking concentration
241 of 10 μM (Supplementary Fig. 1), however BB2-50F did inhibit growth at 100 μM. Restoration
242 of motility following washing after dosage with 10 μM of BB2-50F and supported that this
243 dose was non-lethal and that motility could be reversibly restored. In contrast, HM2-16F at 100
244 μM slowed bacterial growth over the first five hours but was no different from untreated cells
245 after 15 hours (Supplementary Fig. 1). In contrast, BB2-50F was notably toxic at 100 μM,
246 completely inhibiting growth, and likely explaining its consistent anti-motility effect at 100 μM
247 on both stators, in multiple strains, and its irreversible stopping of rotation in the gold bead
248 assay. This indicates a toxic effect of BB2-50F at 100 μM, likely unrelated to any effects on
249 motility proteins. However, it is notable that stopping of rotation in tethered cell assays was
250 seen at a concentration 10-fold lower than this, where no adverse effects on growth were
251 observed in culture (Supplementary Fig. 1).
252 The dose response of phenamil showed an exponential decrease with increased concentration
253 while BB2-50F, in particular, had a sharp effect appearing between 7.5 μM and 10 μM (Fig.
254 1B). These results imply that phenamil and both BB2-50F and HM2-16F have different modes
255 of action: both new compounds stopped rotation in phenamil-resistant stator mutants in *E. coli*,
256 and in native stators in other strains, both Na^+-and H^+-powered. This property represents an
257 improvement over other reported proton-powered motility inhibitors that are effective only in
258 *E. coli* and require high concentrations (up to 600 μM) (42).
259 The mechanism of action of these compounds and the reason(s) for their anti-motility activity
260 across multiple bacterial strains is not clear. The tethered cell assay is a good approach for
261 measuring variations in the response of individual cells to treatment and for initial compound
262 screening, however it does not provide positional information for the rotor or assess
263 performance at low load (43). Most importantly, it is also has the largest surface area in motion,
264 which potentially increases its susceptibility to surface based affects such as increased
265 stickiness. To examine the mechanism of inhibition, and to rule out potentially confounding
266 cell-surface effects that may have influenced earlier experiments using tethered cells, we used
267 a 1 μm polystyrene bead assay (44) to examine the effects of BB2-50F and HM2-16F on
268 rotation. We observed that phenamil in some instances slowed, but did not stop, rotation,
269 whereas BB2-50F and HM2-16F stopped rotation and fixed the location of the bead (Fig. 4).
270 We further examined the effect on statorless constructs (Fig. 4G-I) and noted that phenamil
271 had no effect on rotational diffusion in the absence of stators, whereas BB2-50F andHM2-16F

272 locked free rotational diffusion of the bead. The likely explanation is that phenamil directly
273 associates with the stator complex, reducing active torque generation when bound, and thus
274 has no effect in the absence of stators. In contrast, the two compounds appear to jam the motor
275 or adhere the bead to the cell surface, creating transient pauses, or complete stops at higher
276 concentrations.
277 We used the highest resolution measurement of rotation currently available, a 60-nm gold-
278 nanoparticle affixed directly to a straightened hook (30), to further probe the possible
279 mechanism of action of the compounds. The smaller gold nanoparticle, attached to a
280 straightened hook of ~115 nm length, should not interact with cell surface due to the size of
281 the particle and its distance from the cell membrane. Thus, any observed inhibition would
282 potentially indicate drug binding to the LP ring or bushing of the flagellar motor. However, no
283 inhibition of rotation speed were seen with BB2-50F or HM2-16F at 10 μM in the strains tested
284 using this assay, indicating that the effect of both compounds was likely not due to an on-target
285 interaction with the motor. At high loads there are many stators around a motor, but at low load
286 there should only be a few(31). Our additional measurements of statorless motors at ultra-low
287 load (Fig. 5F & G) saw no change in rotational diffusion in the presence of BB2-50F or HM2-
288 16F at 10 μM. This excludes the possibility that our compounds alter, for example, cell
289 membrane fluidity to interfere with rotation in a stator-dependent manner.
290 At higher concentrations of 100 μM, BB2-50F irreversibly inhibited motility (Supplementary
291 Fig. 4 & 5). At 100 μM, HM2-16F exhibited the full range of effects: from no effect to
292 reversible and irreversible stopping of rotation (Supplementary Fig. 6) This may indicate that
293 100 μM is a threshold concentration at which the adhesion effect can influence the gold bead
294 assay. The use of detergent did not change the potency of BB2-50F and HM2-16F in inhibiting
295 rotation (Supplementary Fig. 7).
296
297 **Conclusions**
298 We have identified two new amiloride analogues with anti-motility effects at 10 μM
299 concentration in multiple bacterial strains. Whilst the exact mechanism of action of each proved
300 elusive, both compounds were able to inhibit motility in known phenamil-resistant mutants.
301 We have used a wide range of biophysical techniques to rule out possible mechanisms of
302 action: these compounds do not target the stators, the LP ring, or the bushing. Future work can
303 integrate fluorescence measurements with these compounds, and other new derivatives, for
304 targeted drug discovery that aids flagellar research and the development of novel
305 antimicrobials.

306

307 **Material and Methods:**

308 **Chemical:**

309 5-(*N*,*N*-hexamethylene)amiloride (HMA) (UOW), HM2-16F (UOW) and BB2-50F (UOW)
310 were synthesised as described previously (23, 24). Phenamil methanesulfonate salt (Sigma-
311 Aldrich), Chloramphenicol (Sigma-Aldrich), Dimethyl sulfoxide (DMSO) (Sigma-Aldrich)
312 and D-Arabinose (Sigma-Aldrich).

313

314 **Bacterial Strains and Plasmids and Growth Conditions**

315 The bacterial strains and plasmids used in this study are shown in full in Supplementary Table
316 1. The primary *E. coli* strains used in this work are SYC35 and RP6894. Pathogenic strains
317 include *Vibrio alginolyticus,* Enterohemorrhagic *Escherichia coli* (EHEC) and Uropathogenic
318 *Escherichia coli* (UPEC). All the strains were cultured in LB broth and LB agar [1% (w/v)
319 Bacto tryptone, 0.5% (w/v) Bacto yeast extract, 0.5% (w/v) NaCl, and 2% (w/v) Bacto agar for
320 solid media] at 37°C. According to the selective antibiotic resistance pattern of the plasmids,
321 chloramphenicol (CAM), ampicillin (AMP) or kanamycin (KAN) were added to a final
322 concentration of 25 µg/mL, 50 µg/mL, and 25 µg/mL, respectively. The *V. alginolyticus* strain,
323 NMB136, was grown in VPG medium (1% (w/v) polypeptone, 0.4% (w/v) K_2HPO_4, 3% (w/v)
324 NaCl, 0.5% (w/v) glycerol) and was washed by TMN85 (85 mM NaCl, 215 mM KCl, 50 mM
325 Tris-HCl (pH 7.5), 5 mM $MgCl_2$, 5 mM glucose) with appropriate inhibitors.

326

327 **Tethered cell assay:**

328 We measured the rotation speed of the test strains in the presence of different concentration of
329 test compounds and control drugs using tethered cell assays following a previous protocol with
330 some modifications (45). *E. coli* strain SYC35 (Δ*motAmotB fliC*^{sticky}) containing plasmids
331 encoding sodium powered PomAPotB (pSHU1234), proton powered MotAMotB (pDB108)
332 and phenamil resistant PonAPotB (pSHU1235, pSHU1236, pSHU1237, and pSHU1249) were
333 inoculated into TB broth [1% (w/v) Bacto tryptone, 0.5% (w/v) NaCl] containing 0.02% (w/v)
334 arabinose and 25 μg/ml chloramphenicol and were grown overnight (17 h) with 180 rpm at 30
335 °C. The overnight cultures were sub-cultured with a 50-fold dilution into fresh TB broth and
336 incubated for 5 h with 180 rpm at 30°C to get more motile cells. At OD_{600} ~0.80, the flagella
337 of the cells were sheared by passing the culture multiple times (~35) through a 26G needle
338 syringe. After shearing the flagella, the cells were washed three times with motility buffer [10
339 mM potassium-phosphate, 10 mM lactic acid, 100 mM NaCl, and 0.1 mM EDTA, pH 7.0].
340 Cells were then attached on tunnel slides and washed sequentially with motility buffer that
341 contained different concentration test compounds (0, 1, 2.5, 5, 7.5, 10, and 100 μM). According
342 to the experiment purpose we used different concentrations NaCl in the motility buffer. The
343 rotational speed of the cells was observed using phase-contrast microscopy (Nikon) and was
344 recorded at 20 frames per second (FPS) through the 40X objective with a camera (Chameleon3
345 CM3, Point Grey Research). Rotational motion of the cells was analysed using Lab view 2019
346 software (National Instruments).

347

348 **Free swimming assay:**

349 We measured the swimming speed of the test strains in the presence drugs following a previous
350 protocol (46). Briefly, the *E. coli* strains were inoculated into TB broth (1% (w/v) Bacto
351 tryptone, 0.5% (w/v) NaCl) with additional 0.02% (w/v) arabinose and 25 μg/ml
352 chloramphenicol (where required) and were grown overnight (17 h) with 180 rpm at 30°C.
353 NMB136 cells were inoculated in VPG medium (1% polypeptone, 0.4% K_2HPO_4, 3% NaCl,
354 0.5% glycerol) and were grown overnight with 180 rpm at 30°C. For *E. coli* strains, overnight
355 cultures were subcultured with a 50-fold dilution into fresh TB broth and incubated for 5 h with
356 180 rpm at 30°C. At OD_{600} ~0.80, the cells were washed once with motility buffer (10 mM
357 potassium-phosphate, 10 mM lactic acid, 100 mM NaCl, and 0.1 mM EDTA, pH 7.0). For
358 NMB136 cells, overnight cultures were subcultured with a 100-fold dilution into fresh VPG
359 medium and incubated for 3 h with 180 rpm at 30°C. At OD600 ~1.0, the cells were washed

360 twice with TMN85 (85 mM NaCl, 215 mM KCl, 50 mM Tris-HCl (pH 7.5), 5 mM $MgCl_2$, 5
361 mM glucose). Then, cell suspensions were mixed with equivalent volume of the inhibitor
362 solution (at 2x of the intended final concentration) to achieve a final concentration of 10 μM
363 or 100 μM of compound. Finally, 15 μL of cell-inhibitor mixtures were added to the tunnel
364 slide and the swimming speed of the cells was observed using phase-contrast microscopy. For
365 *E. coli* strains: 20 s was recorded at 20 frames per second (fps) through a 20x objective (Nikon)
366 with a camera (Chameleon3 CM3, Point Grey Research). For NMB136 cells: 10 s was recorded
367 at 60 fps through a 20x objective (Olympus) with a camera (DMK21AU618, IMAGING
368 SOURCE). The swimming speed of the cells in both cases was analysed using LabVIEW 2019
369 software (National Instruments).
370
371 **Growth Curve Assays**
372 Growth assays were performed in the presence of predetermined concentration of test
373 compound to evaluate the effect of the compounds on bacterial growth following the previous
374 protocol (47) with slight modification. *E. coli* strain SYC35 transformed with sodium powered
375 (PomAPotB) and protonpowered (MotAMotB) was used. Briefly, overnight cultures of the test
376 strains with OD_{600} 1.0 were diluted 1:100 in 96-well plates (Corning) with fresh LB broth
377 containing different concentrations of HM2-16F and BB2-50F and incubated at 37°C. Plasmid
378 containing strains (pSHU1234 and pDB-108) were grown in presence of 0.02% (w/v) arabinose
379 and 25 μg/mL chloramphenicol, whereas EHEC and UPEC were grown in LB without
380 arabinose or antibiotic. The OD_{600} were measured in a microplate reader (FLUOstar OPTIMA,
381 BMG LABTECH) every hour for 15 h with a brief shaking interval before each measurement.
382 Measurements in 10 μM were repeated and averaged over three measurements, measurements
383 for 100 μM were repeated and averaged over six measurements.
384

385 **Polystyrene bead assay:**

386 Briefly, *E. coli* strain JHC36 (Δ*motAmotB* Δ*cheY fliC*^{sticky}) transformed with plasmids encoding
387 sodium powered (PomAPotB) and proton powered (MotAMotB) was grown overnight in TB
388 broth and then sub-cultured with a 50-fold dilution into fresh TB broth and incubated for 5 h
389 with 180 rpm at 30°C to get more motile cells. At OD_{600} ~0.80, the flagella of the cells were
390 sheared by passing the culture multiple times (~35) through a 26G needle syringe. After
391 shearing the flagella, the cells were washed three times with motility buffer [10 mM potassium-
392 phosphate, 85 mM NaCl, and 0.1 mM EDTA, 1% DMSO, pH 7.0]. Then, the glass slide was
393 coated with poly-L-lysine (PLL) (Sigma Aldrich) and incubated for 10 mins and washed with
394 motility buffer and flushed with 1 µm polystyrene bead (Polysciences, Inc) solution. The
395 sample was then washed with motility buffer containing test compound (10 and 100 µM) and
396 the rotational speed was recorded and analyzed using Lab view 2019 software (National
397 Instruments).

398

399 **Gold-nanoparticle assay:**

400 We used the 60 nm gold-nanoparticle assay to get the more accurate flagellar rotation speed at
401 lowered load using the previous protocol (30) with slight modification. Briefly, the SHU174
402 *E. coli* (Δ*motAmotB* Δ*fliC* Δ*cheY flgE*$_{+GSS+3Cys}$ *fliK2798*) containing plasmids encoding stators
403 was grown and washed with KPi buffer (10 mM potassium-phosphate, 0.1 mM EDTA, pH 7.0)
404 and prepared as a cell suspension. The cell suspension was later added to the precipitation of
405 gold nano particle (BBI solutions) and incubated for 30 min. After incubation, the cell mixture
406 was washed with KPi buffer and put into PLL coated glass chamber. The sample was then
407 washed with motility buffer (10 mM potassium-phosphate, 10 mM lactate-Na, 67 mM NaCl,
408 0.1 mM EDTA, 1% DMSO, pH 7.0) containing test compound (10 and 100 µM) and the
409 rotational speed was recorded and analyzed using LabVIEW 2019 software (National
410 Instruments).

411

412 **Evaluation of fluorescence property of HM2-16F:**

413 The fluorescence of HM2-16F was analysed using fluorescence microscopy. The emission and
414 excitation spectra of the drug was measured using a spectrophotometer (Cary Eclipse). Briefly,
415 the overnight culture of *E. coli* SYC35 strain transformed with pSHU1234 was prepared and
416 washed with motility buffer. Later, the cell suspension was added to PLL-coated glass slide
417 and incubated for 10 mins and again washed with motility buffer. Cells were treated with test
418 compounds by washing with test compound (10 and 100 µM) containing motility buffer.

419 Finally, drug treated cells were imaged in epifluorescence mode using a Elyra Microscope
420 (Zeiss) using a Plan-Apochromat 63x/1.40 Oil DIC M27 objective, 405 nm illumination and
421 BP495-575 + L750 filter sets. Lifetime imaging was executed on Picoquant MicroTime 200
422 STED equipped with a PMA Hybrid Series Hybrid Photomultiplier Detector. Illumination was
423 provided by 405 nm laser (Diode 450), with a 60x/1.2 UPlanSApo Water Objective.
424

425 **AUTHOR CONTRIBUTIONS**

426 MIM, JB, TI, PR, BJB and MABB designed and executed experiments in, medicinal chemistry,
427 microbiology, microscopy, and rotational measurement. MIM and JL, MJK, BJB, MABB
428 executed initial compound screening. TI and YS designed and executed experiments in
429 rotational measurement with polystyrene beads and gold nanoparticles. MABB and BJB
430 supervised the design, execution and writing of the project. All authors contributed to writing
431 and revision of the manuscript.
432

433 **ACKNOWLEDGEMENTS**

434 We would like to thank Tohru Minamino, Yong-Suk Che, Myu Yoshida and Rie Ito for helping
435 a construction of strains and plasmids. We would like to thank Jai Tree for providing the EHEC
436 and UPEC strains and thank Seiji Kojima and Michio Homma for providing the *V. alginolyticus*
437 strain.

438

439 **FUNDING**

440 MJK was supported by Australian National Health and Medical Research Council (NHMRC)
441 Project Grant (APP1100432). YS was supported by JSPS KAKENHI (JP18H02475 and
442 JP20K06564), MEXT KAKENHI (JP19H05404) and Takeda Science Foundation. BJB
443 acknowledges salary support from the Illawarra Cancer Carers. MABB was supported by a
444 UNSW Scientia Research Fellowship, a CSIRO Synthetic Biology Future Science Platform
445 2018 Project Grant, and ARC Discovery Project DP190100497.
446

447 **References:**

448 1. Duan Q, Zhou M, Zhu L, Zhu G. 2013. Flagella and bacterial pathogenicity. J Basic
449 Microbiol 53:1–8.

450 2. Armitage JP. 2007. Bacterial TaxisEncyclopedia of Life Sciences.

451 3. Berg HC. 2008. E. coli in Motion. Springer Science & Business Media.

452 4. Sowa Y, Berry RM. 2008. Bacterial flagellar motor. Q Rev Biophys 41:103–132.

453 5. Xiu P, Liu R, Zhang D, Sun C. 2017. Pumilacidin-Like Lipopeptides Derived from
454 Marine Bacterium Bacillus sp. Strain 176 Suppress the Motility of *Vibrio alginolyticus*.
455 Appl Environ Microbiol 83.

456 6. Yang Q, Defoirdt T. 2015. Quorum sensing positively regulates flagellar motility in
457 pathogenic *Vibrio harveyi*. Environ Microbiol 17:960–968.

458 7. Black RE, Levine MM, Clements ML, Hughes TP, Blaser MJ. 1988. Experimental
459 Campylobacter jejuni Infection in Humans. J Infect Dis 157:472–479.

460 8. Josenhans C, Suerbaum S. 2002. The role of motility as a virulence factor in bacteria.
461 Int J Med Microbiol 291:605–614.

462 9. Kao C-Y, Sheu B-S, Wu J-J. 2016. Helicobacter pylori infection: An overview of
463 bacterial virulence factors and pathogenesis. Biomed J 39:14–23.

464 10. Arslan-Aydoğdu EÖ, Kimiran A. 2018. An investigation of virulence factors of
465 *Legionella pneumophila* environmental isolates. Braz J Microbiol 49:189–199.

466 11. Kao CY, Lin WH, Tseng CC, Wu AB, Wang MC, Wu JJ. 2014. The complex interplay
467 among bacterial motility and virulence factors in different *Escherichia coli* infections.
468 Eur J Clin Microbiol Infect Dis 33:2157–2162.

469 12. Drake D, Montie TC. 1988. Flagella, Motility and Invasive Virulence of *Pseudomonas*
470 *aeruginosa*. Microbiology, 134:43–52.

471 13. Allen-Vercoe E, Sayers AR, Woodward MJ. 1999. Virulence of *Salmonella enterica*
472 serotype Enteritidis aflagellate and afimbriate mutants in a day-old chick model.
473 Epidemiol Infect 122:395–402.

474 14. McCarter LL. 2001. Polar Flagellar Motility of the Vibrionaceae. Microbiol Mol Biol
475 Rev 65:445–462.

476 15. Simchowitz L, Cragoe EJ. 1986. Inhibition of chemotactic factor-activated Na+/H+
477 exchange in human neutrophils by analogues of amiloride: structure-activity
478 relationships in the amiloride series. Mol Pharmacol 30:112–120.

479 16. Sugiyama S, Cragoe EJ, Imae Y. 1988. Amiloride, a specific inhibitor for the Na+-
480 driven flagellar motors of alkalophilic Bacillus. J Biol Chem 263:8215–8219.

481 17. Atsumi T, Sugiyama S, Cragoe EJ, Imae Y. 1990. Specific inhibition of the Na(+)-
482 driven flagellar motors of alkalophilic Bacillus strains by the amiloride analog
483 phenamil. J Bacteriol 172:1634–1639.

484 18. Guia A, Leblanc N, Bose R. 1995. Effects of phenamil on potassium and calcium
485 channels of guinea pig ventricular myocytes. J Pharmacol Exp Ther 274:649–656.

486 19. Kojima S, Asai Y, Atsumi T, Kawagishi I, Homma M. 1999. Na+-driven flagellar motor
487 resistant to phenamil, an amiloride analog, caused by mutations in putative channel
488 components. J Mol Biol 285:1537–1547.

489 20. Jaques S, Kim Y-K, McCarter LL. 1999. Mutations conferring resistance to phenamil
490 and amiloride, inhibitors of sodium-driven motility of Vibrio parahaemolyticus. Proc
491 Natl Acad Sci 96:5740–5745.

492 21. Ishida T, Ito R, Clark J, Matzke NJ, Sowa Y, Baker MAB. 2019. Sodium-powered
493 stators of the bacterial flagellar motor can generate torque in the presence of phenamil
494 with mutations near the peptidoglycan-binding region. Mol Microbiol 111:1689–1699.

495 22. Terada H. 1990. Uncouplers of oxidative phosphorylation. Environ Health Perspect
496 87:213–218.

497 23. Buckley BJ, Aboelela A, Minaei E, Jiang LX, Xu Z, Ali U, Fildes K, Cheung C-Y,
498 Cook SM, Johnson DC, Bachovchin DA, Cook GM, Apte M, Huang M, Ranson M,
499 Kelso MJ. 2018. 6-Substituted Hexamethylene Amiloride (HMA) Derivatives as Potent
500 and Selective Inhibitors of the Human Urokinase Plasminogen Activator for Use in
501 Cancer. J Med Chem 61:8299–8320.

502 24. Buckley BJ, Majed H, Aboelela A, Minaei E, Jiang L, Fildes K, Cheung C-Y, Johnson
503 D, Bachovchin D, Cook GM, Huang M, Ranson M, Kelso MJ. 2019. 6-Substituted
504 amiloride derivatives as inhibitors of the urokinase-type plasminogen activator for use
505 in metastatic disease. Bioorg Med Chem Lett 29:126753.

506 25. Nishiyama M, Sowa Y. 2012. Microscopic Analysis of Bacterial Motility at High
507 Pressure. Biophys J 102:1872–1880.

508 26. Tree JJ, Ulett GC, Ong C-LY, Trott DJ, McEwan AG, Schembri MA. 2008. Trade-off
509 between iron uptake and protection against oxidative stress: deletion of cueO promotes
510 uropathogenic Escherichia coli virulence in a mouse model of urinary tract infection. J
511 Bacteriol 190:6909–6912.

512 27. Sy BM, Lan R, Tree JJ. 2020. Early termination of the Shiga toxin transcript generates a
513 regulatory small RNA. Proc Natl Acad Sci U S A 117:25055–25065.

514 28. Dahan S, Knutton S, Shaw RK, Crepin VF, Dougan G, Frankel G. 2004. Transcriptome
515 of enterohemorrhagic Escherichia coli O157 adhering to eukaryotic plasma membranes.
516 Infect Immun 72:5452–5459.

517 29. Kojima S, Atsumi T, Muramoto K, Kudo S, Kawagishi I, Homma M. 1997. Vibrio
518 alginolyticus mutants resistant to phenamil, a specific inhibitor of the sodium-driven
519 flagellar motor. J Mol Biol 265:310–318.

520 30. Nakamura S, Hanaizumi Y, Morimoto YV, Inoue Y, Erhardt M, Minamino T, Namba
521 K. 2020. Direct observation of speed fluctuations of flagellar motor rotation at
522 extremely low load close to zero. Mol Microbiol 113:755–765.

523 31. Nord AL, Sowa Y, Steel BC, Lo C-J, Berry RM. 2017. Speed of the bacterial flagellar
524 motor near zero load depends on the number of stator units. Proc Natl Acad Sci
525 114:11603–11608.

526 32. Wang B, Zhang R, Yuan J. 2017. Limiting (zero-load) speed of the rotary motor of
527 Escherichia coli is independent of the number of torque-generating units. Proc Natl
528 Acad Sci 114:12478–12482.

529 33. Soman V, Malik KS, Nath S, Elangovan R. 2020. Effect of cell size and tethering
530 geometry on rotation rate, torque, and rotational bias of E.coli cells. bioRxiv
531 2020.05.11.088310.

532 34. Grognot M, Taute KM. 2021. A multiscale 3D chemotaxis assay reveals bacterial
533 navigation mechanisms. Commun Biol 4:1–8.

534 35. Allen RC, Popat R, Diggle SP, Brown SP. 2014. Targeting virulence: can we make
535 evolution-proof drugs? 4. Nat Rev Microbiol 12:300–308.

536 36. Barczak AK, Hung DT. 2009. Productive steps toward an antimicrobial targeting
537 virulence. Curr Opin Microbiol 12:490–496.

538 37. van Alphen LB, Burt SA, Veenendaal AKJ, Bleumink-Pluym NMC, van Putten JPM.
539 2012. The natural antimicrobial carvacrol inhibits Campylobacter jejuni motility and
540 infection of epithelial cells. PloS One 7:e45343.

541 38. Mohr K. 1993. Amiloride and Its Analogs Unique Cation Transport Inhibitors. Edward
542 J. Cragoe jr., Thomas R. Kleyman, Louis Simchowitz. VCH Weinheim — New York —
543 Basel — Cambridge — Tokyo. Date of publication: December 1992. XV, 388 pages. 62
544 figures. 25 tables. DM 189,—, £ 78,—. Pharm Unserer Zeit 22:273–273.

545 39. McCarter LL. 2004. Dual Flagellar Systems Enable Motility under Different
546 Circumstances. Microb Physiol 7:18–29.

547 40. Atsumi T, Yoshimura F, Sugiyama S. 2006. Arginine inhibits Na-driven flagellar
548 motors of alkaliphilic Bacillus. FEMS Microbiol Lett 256:224–228.

549 41. Stone MRL, Butler MS, Phetsang W, Cooper MA, Blaskovich MAT. 2018. Fluorescent
550 Antibiotics: New Research Tools to Fight Antibiotic Resistance. Trends Biotechnol
551 36:523–536.

552 42. Adams LA, Sharma P, Mohanty B, Ilyichova OV, Mulcair MD, Williams ML, Gleeson
553 EC, Totsika M, Doak BC, Caria S, Rimmer K, Horne J, Shouldice SR, Vazirani M,
554 Headey SJ, Plumb BR, Martin JL, Heras B, Simpson JS, Scanlon MJ. 2015. Application
555 of Fragment-Based Screening to the Design of Inhibitors of Escherichia coli DsbA.
556 Angew Chem Int Ed 54:2179–2184.

557 43. Nirody JA, Sun Y-R, Lo C-J. 2017. The biophysicist's guide to the bacterial flagellar
558 motor. Adv Phys X 2:324–343.

559 44. Kasai T, Sowa Y. 2017. Measurements of the Rotation of the Flagellar Motor by Bead
560 Assay. Methods Mol Biol Clifton NJ 1593:185–192.

561 45. Sowa Y, Homma M, Ishijima A, Berry RM. 2014. Hybrid-fuel bacterial flagellar motors
562 in Escherichia coli. Proc Natl Acad Sci 111:3436–3441.

563 46. Morimoto YV, Namba K, Minamino T. 2017. Measurements of Free-swimming Speed
564 of Motile Salmonella Cells in Liquid Media. Bio-Protoc 7:e2093–e2093.

565 47. Islam MI, Lin A, Lai Y-W, Matzke NJ, Baker MAB. 2020. Ancestral Sequence
566 Reconstructions of MotB Are Proton-Motile and Require MotA for Motility. Front
567 Microbiol 11.

568

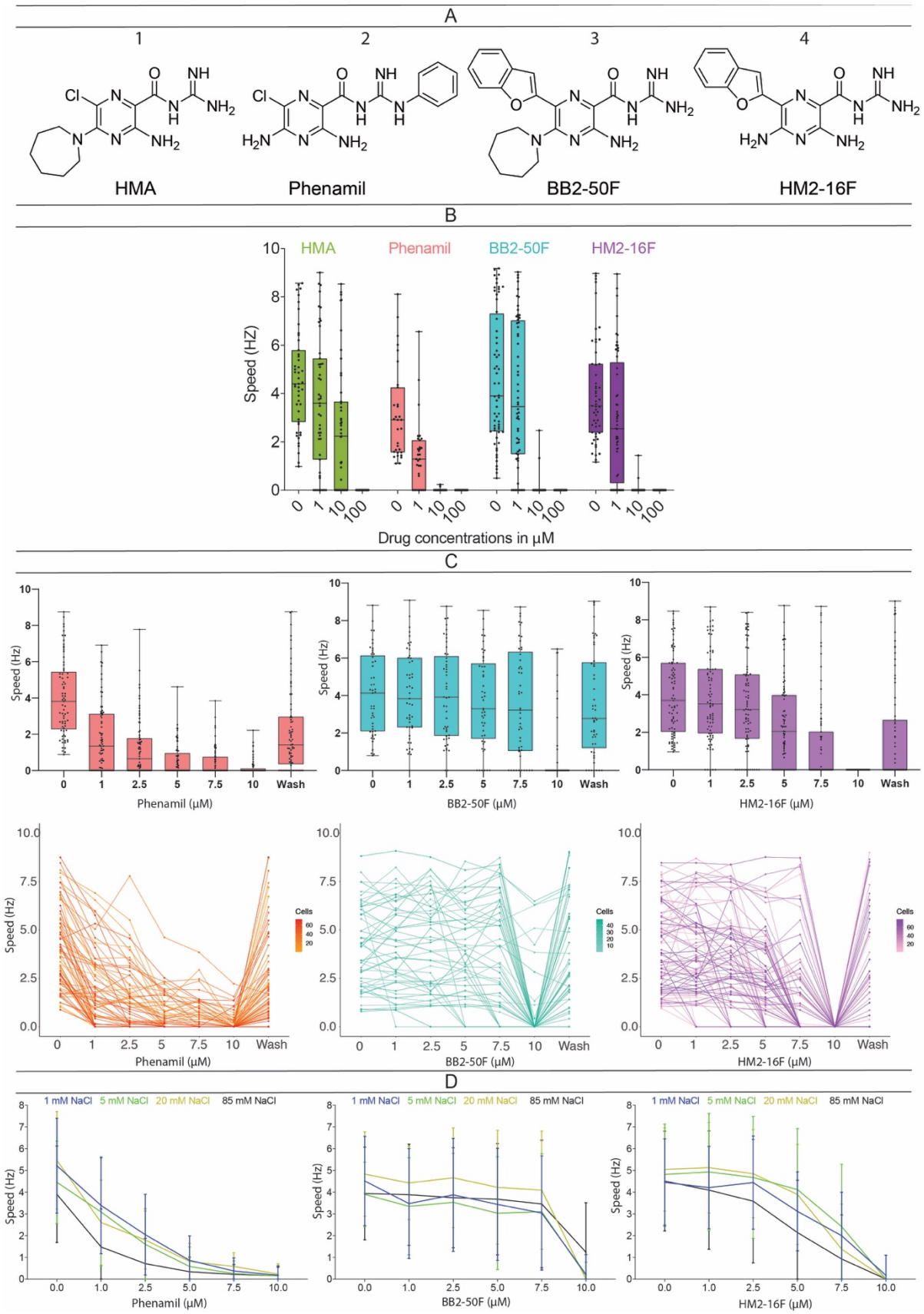

Fig. 1: Structures and effects of compounds on bacterial rotation in tethered cell assays. **(A)** Chemical structures of controls 5-*N,N*-(hexamethylene)amiloride (HMA) and phenamil

572 and test compounds BB2-50F and HM2-16F. **(B)** Tethered cell rotation speed (Hz) after
573 treatment with drugs (μM). Cells were *E. coli* SYC35 strain with PomAPotB stators
574 (pSHU1234). Cells were treated with 0, 1, 10 and 100 μM of each compound. Boxes represent
575 the 25th and 75th percentile, with median indicated by dividing line. Whiskers cover the full
576 range from minimum to maximum
577 ($n \geq 30$). The lime green bar = HMA, salmon = phenamil, blue = BB2-50F and violet = HM2-
578 16F. **(C)** Dose characterisation of compounds. Cells were treated with 0, 1, 2.5, 5, 7.5 and 10
579 μM of each compound. The line graphs (bottom) indicate the tracking of individual cells'
580 change in rotation speed. **(D)** Effects of sodium concentration ([Na^+]) on inhibitory activity.
581 Cells were treated with 0, 1, 2.5, 5, 7.5 and 10 μM drugs diluted in motility buffer containing
582 different Na^+ concentrations (1, 5, 20 and 85 mM). Total ionic concentration was held constant
583 and balanced with 85, 80, 65 and 0 mM KCl respectively.

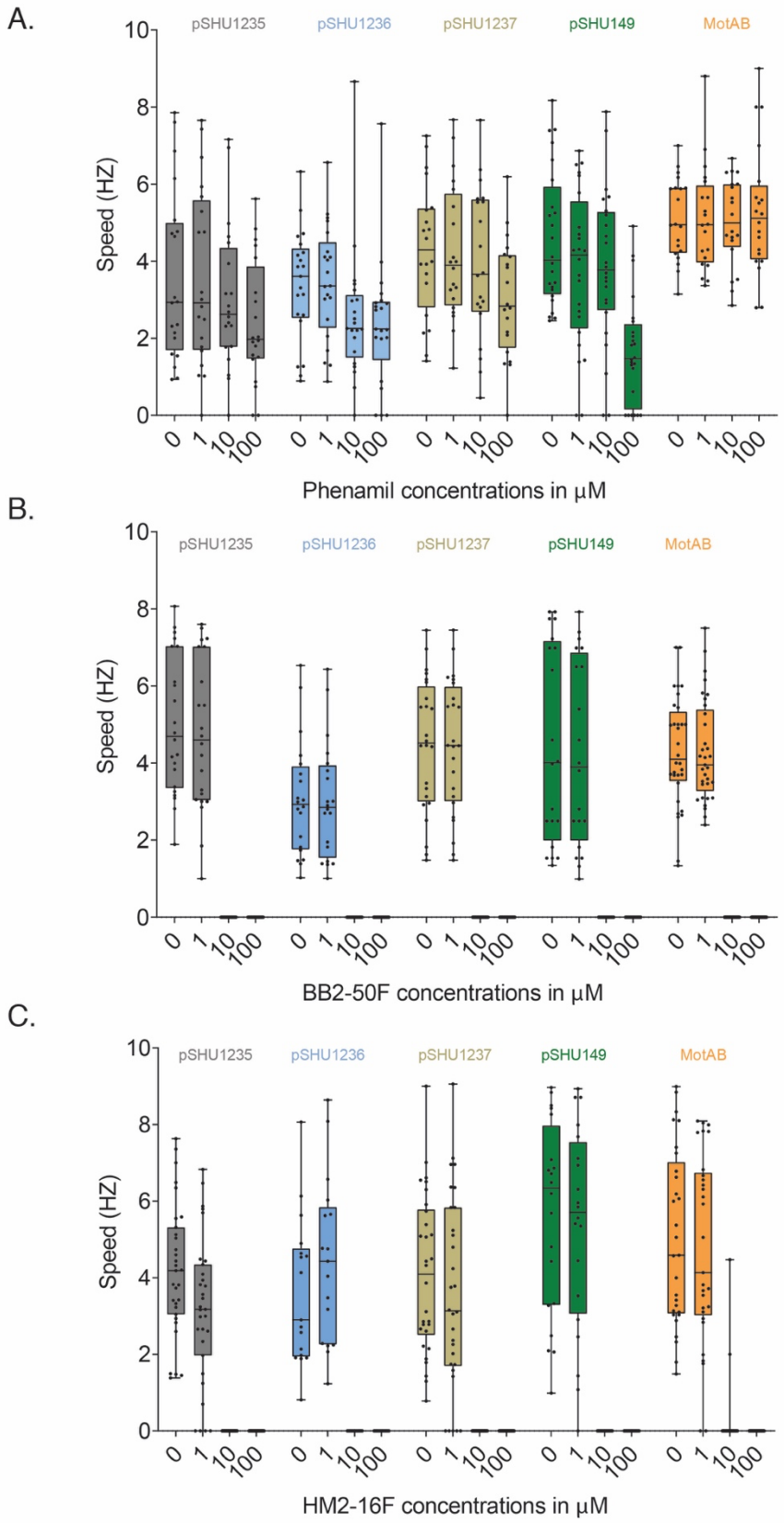
A.
pSHU1235
pSHU1236
pSHU1237
pSHU149
MotAB
Speed (HZ)
Phenamil concentrations in µM
B.
BB2-50F concentrations in µM
C.
HM2-16F concentrations in µM

584

585

586 **Fig. 2:** Activity of compounds against phenamil-resistant stators and proton-powered
587 MotAMotB. Tethered cell speed (Hz) in response to 0, 1, 10, and 100 µM of: **A)** phenamil, **(B)**
588 BB2-50F and (**C**) HM2-16F. Cell used for all assays were *E. coli* SYC35 with
589 PomA(D148Y)/PotB (pSHU1235), PomA/PotB(P16S) (pSHU1236),
590 PomA(D148Y)/PotB (P16S) (pSHU1237), PomA/PotB(F22Y/L28Q) (pSHU149) and
591 MotAMotB(pDB-108), respectively. Boxes represent the 25th and 75th percentile, with median
592 indicated by dividing line. Whiskers depict the full range from minimum to maximum ($n \geq 20$).

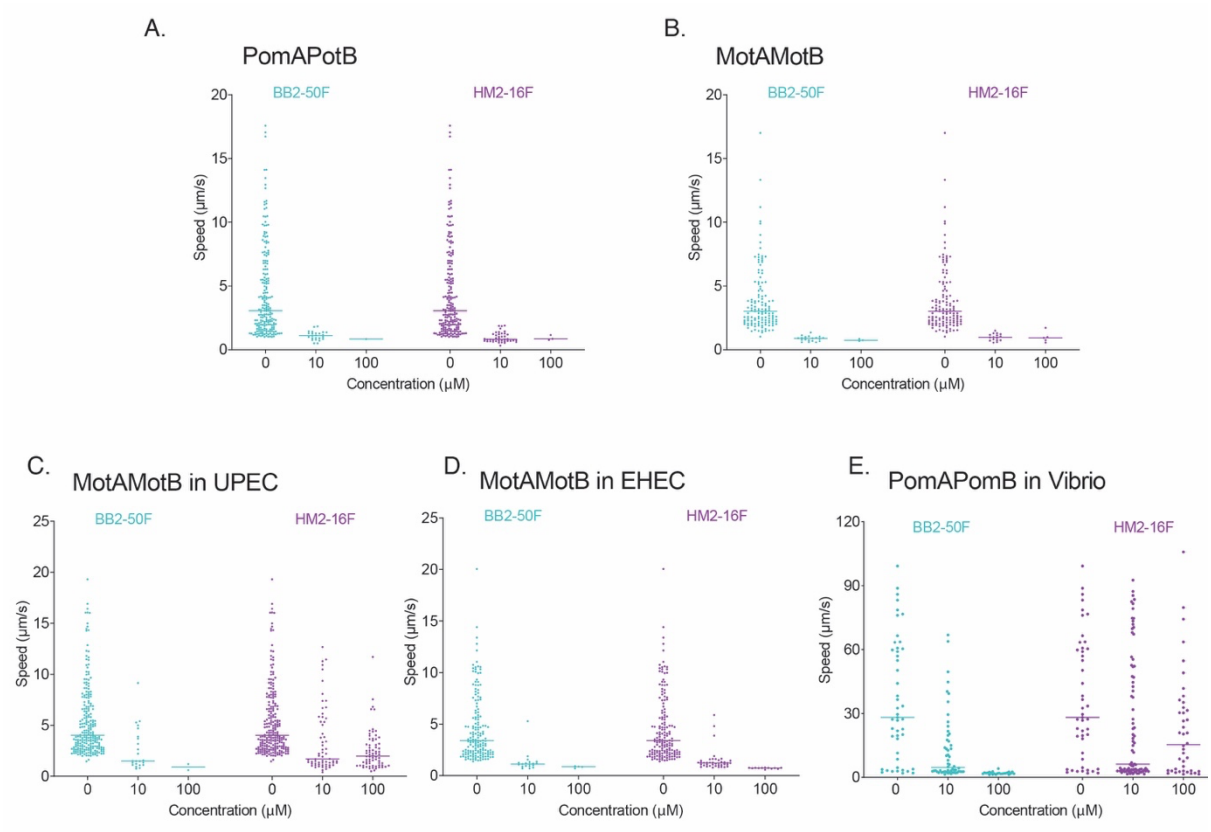

593

594 **Fig. 3**: Inhibition of swimming speed by BB2-50F and HM2-16F. Bacterial swimming speed
595 was measured by tracking individual cells using videography in the presence of different
596 concentrations (0, 10, 100 μM) of each compound. Swimming speed of: **(A)** PomAPotB
597 expressed via plasmid in Δ*motAB* strain, **(B)** MotAMotB expressed via plasmid in Δ*motAB*
598 strain, **(C)** MotAMotB in uropathogenic *Escherichia coli* (UPEC) and **(D)** MotAMotB in
599 enterohemorrhagic *Escherichia coli* (EHEC), and **(E)** PomAPomB in *Vibrio alginolyticus,* all
600 following wash with drug. Speeds of individual cells shown in μm/s with the scattered plots,
601 median speed indicated by line (n ≥ 30).

602

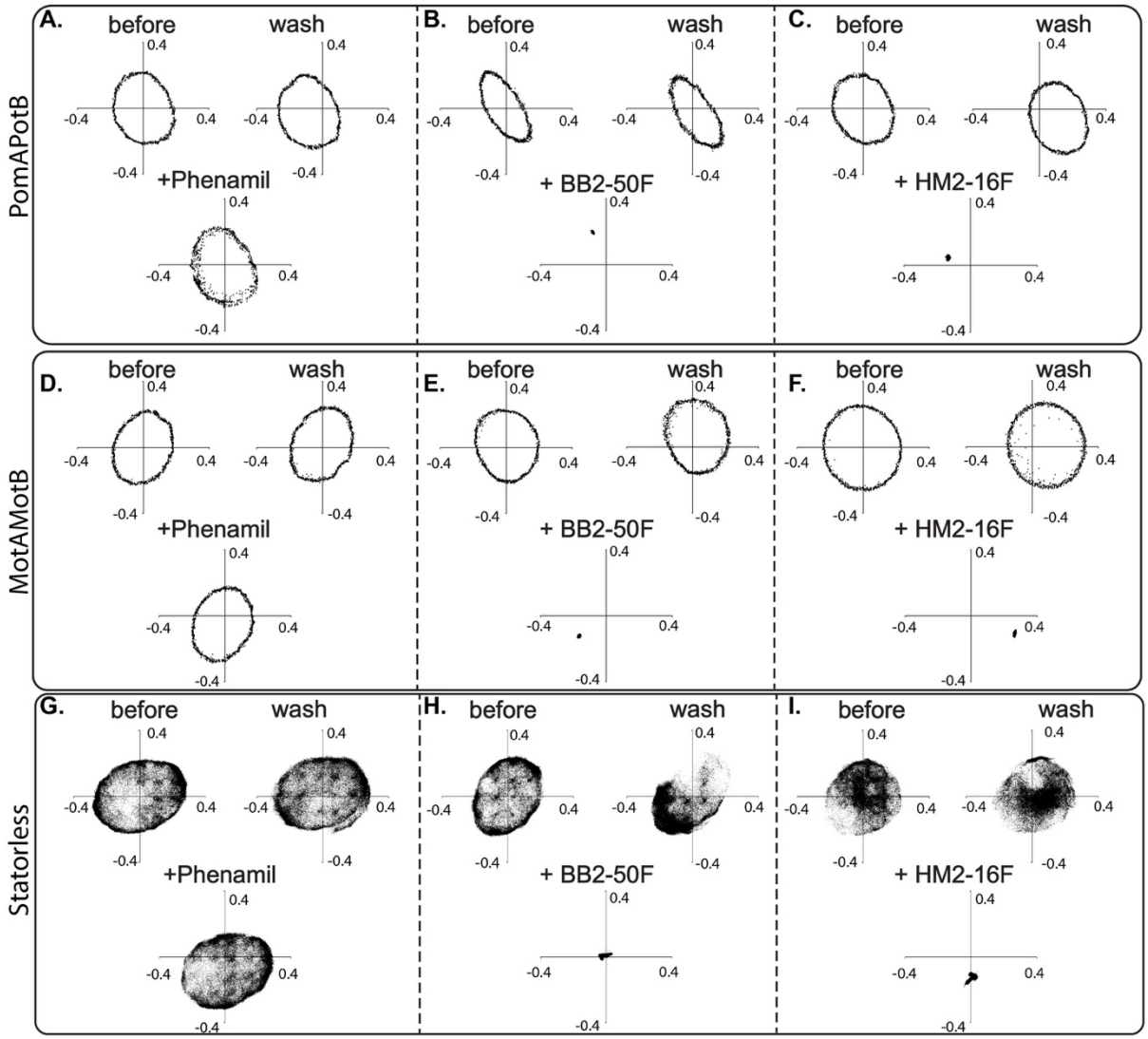

Fig. 4: Bead assay results for phenamil, BB2-50F and HM2-16F. (top) 1 µm Polystyrene bead assay in *E. coli* strain JHC36 with plasmid expressing PomAPotB stator (pSHU1234) in presence of (A) phenamil, (B) BB2-50F and (C) HM2-16F. Each panel shows three X-Y scatter plots (over 1 s) of the position a bead attached to the rotating flagellar filament of a single cell before exposure to drug, after exposure to drug, and after wash to remove drug. Raw speed vs time and XY vs time plots shown in Supplementary Fig. 2. **(middle)** Bead assay in *E. coli* strain JHC36 with plasmid expressing MotAMotB stator in presence of (D) phenamil, (E) BB2-50F and (F) HM2-16F. **(Bottom)** X-Y position (over 60 s) for *E. coli* strain JHC36 with no stators expressed. The Brownian diffusion of the bead for 60-120 s is shown before and after treatment with (G) phenamil, (H) BB2-50F and (I) HM2-16F, respectively. All drugs washed in as 50 µL of 10 µM drug, washed out with 200 µL of 85MTB. All lengths in µm.

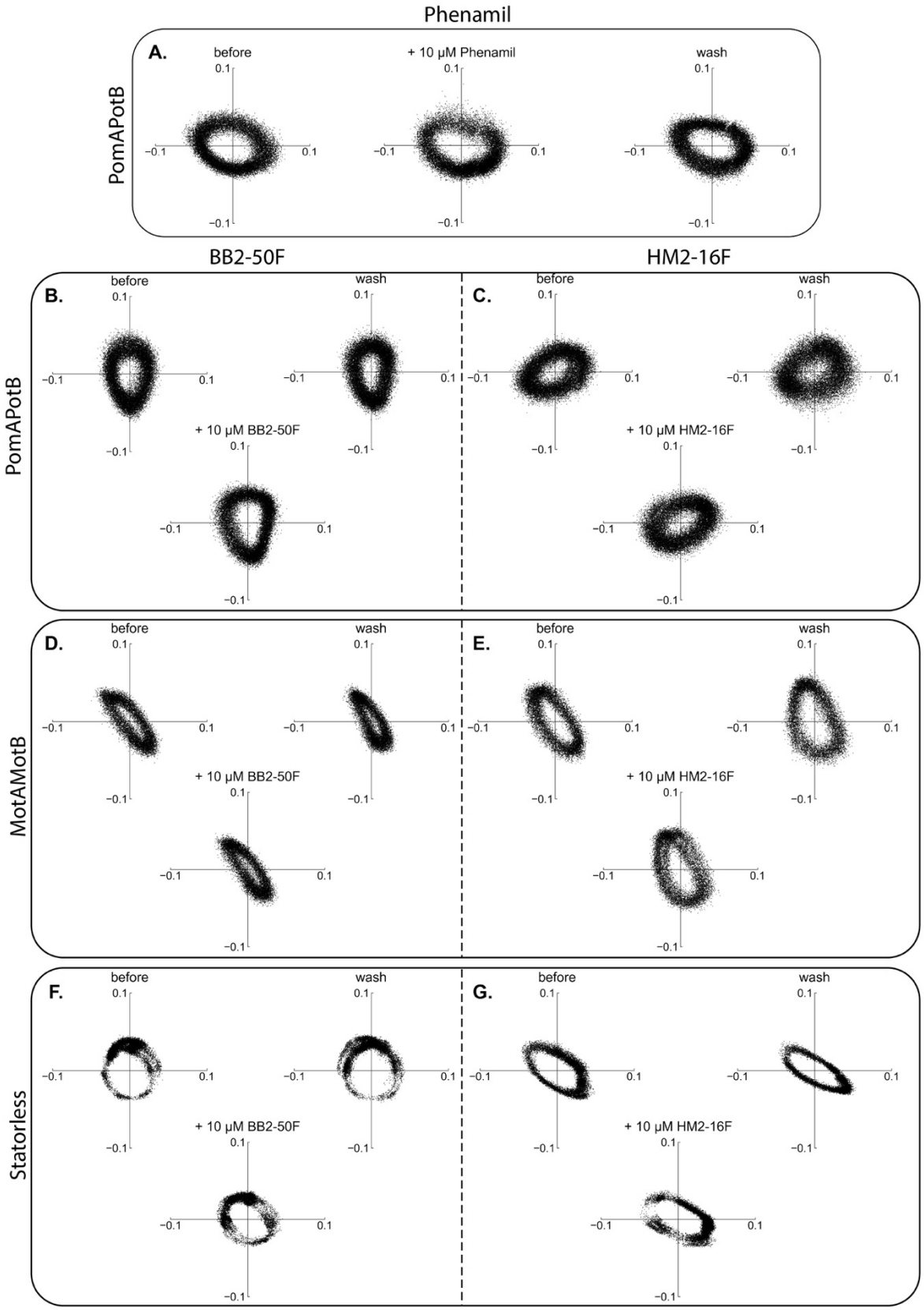

616

617 **Fig. 5: Gold bead nanoparticle assay results phenamil, BB2-50F and HM2-16F.** Gold
618 nanoparticle assay was performed in SHU174 *E. coli* strain in presence of 10 μM BB2-50F

619 (left) and HM2-16F (right) for both PomAPotB and MotAMotB stators, with phenamil action
620 on PomAPotB as a positive control (top). (A) Positive control for 10 μM phenamil against
621 rotation driven by PomAPotB. Rotation of full circles is maintained, with slowing of cell speed
622 speed vs time shown in Supplementary Fig. 4). 10 μM of BB2-50F (B) and HM2-16F (C)
623 acting on PomAPotB stators has no effect or gold bead rotation. 10 μM of BB2-50F (D) and
624 HM2-16F (E) acting on MotAMotB has no effect on gold bead rotation. 10 μM of BB2-50F
625 (F) and HM2-16F (G) acting on statorless cells. Rotational diffusion of gold bead tracks circles
626 and is not impeded. Data for PomAPotB, MotAMotB and statorless strainst against 100 μM of
627 compound is shown in Supplementary Fig. 5 & 6. All lengths in μm.